Ultra-Short Pulse

Executive Summary

Here, we investigate the use of femtosecond laser pulses, or ultrashort pulses (USPs), as a means of stimulating and detecting potential AHE events. The primary difference for this stimulation method is that it is *non-thermal* in nature: excitation occurs at timescales faster than atomic motion. To rigorously test the stimulation conditions, we vary the wavelength from UV through THz, spanning various material processes ranging from deep electron excitation to direct phonon interaction and vary the pulse intensity from well-below damage threshold to intensities in which high-energy particles are observed to be emitted from the material system. These stimulation methods are aided by the use of Transient Reflectivity (TR) as a means of femtosecond-resolution probing of temperature and thus potential AHE events, as well as Archaeology-type samples to allow for single event sensitivity. While PdD_x and PdH_x demonstrate interesting behavior relative to their unloaded counterpart, these studies provide clear evidence that AHE is not occurring due to USP stimulation.

Ultra-short pulses: Stimulation and detection of AHE

A plethora of hypotheses on the "mechanism" for inducing nuclear reactions within a solid-state material exist within LENR literature. However, these can nearly all be summarized within two broad categories: Electron-driven events or lattice-driven events. In the former case, one example theory is that the electrons in the material can "screen" the native repulsion that occurs between two deuterons (notably, this is a well-understood process in both solid-state physics as well as high-energy physics), with the general idea being that two positively charged deuterons will be brought together through their equal attraction to a centering electron and thus reach a proximity in which fusion occurs. In the latter case for lattice-driven reactions, one may hypothesize examples such as the potential for deuterons to simultaneously "hop" into an identical position within a lattice. As this lattice position is stable and is a strong local minimum within the energy landscape, the deuterons may be capable of reaching proximities for fusion to occur. However, direct manipulation of either parameter is a non-trivial task.

Few methods exist of tuning electronic states or the local lattice environment without corresponding changes to the host material. Generally, meaningful changes to electronic states require dopants, which, in turn, also affects the surrounding lattice. Similarly, to induce something akin to the hopping-rate or diffusivity of atoms within a material, one must distort the lattice itself. In other words, it is generally difficult to modify the conditions surrounding a deuteron within a lattice without significant lattice distortion in itself. This nuanced complication can mean that our

assumptions of the *initial* lattice state, and hopping within that initial state, are incorrect: During hopping, the "lattice state" may be modified, leading to difficult interpretations.

One notable method that can achieve such changes to either the electronic or lattice-based states is via optical stimulation. In fact, this is the *primary* method of inducing changes to either state independently of the other: Electrons can shift energy levels simply by absorption and emission of light, and the hopping rate is dictated by vibrational states (i.e., phonons) which, at least in some cases, can be IR-active and thus "stimulated" by light. However, *meaningful* changes will not be expected for low light intensities; thermal radiation persists at nearly all infrared wavelengths continuously at room temperature and yet we have not observed lattices undergoing constant fusion (in fact, the power emitted by thermal radiation from a human body at room temperature [~1,000 Watts] is significantly higher than most reports of anomalous heat!). A similar argument can be made for electronic states: Both inter- and intraband transitions can occur continuously in a metal that is irradiated by even standard room lights, with both transitions having non-zero probabilities (in most materials) at room temperature simply due to Fermi-Dirac statistics. In other words, to expect *meaningful* modification of the states of interest, one likely requires a source of *intense* light.

Ultrashort pulses (USPs) of light can overcome these limitations and provide a unique method of both stimulation and detection. From a stimulation perspective, one can envision multiple scenarios that may lead to induced nuclear reactions. For example, USPs can deliver significant amounts of energy on timescales faster than atomic motion can occur (GW power densities in a single pulse). For context, the femtosecond lasers at Callisto Research can deliver mJ energy levels per-pulse in under 50 femtoseconds: providing a lower limit on the *instantaneous* power of 1 mJ/50 femtoseconds ~ 20 GW. This power is equivalent to *twenty* nuclear power plants all delivered within a single pulse. In other words, a single laser pulse can deliver as much power as the world's largest power plant but all delivered into a single material, thus providing access to highly energetic and strongly non-equilibrium lattice conditions.

From a detection perspective, these USPs have multiple advantages. First, optical probing has the benefit of being a "stand-off" technique – difficult micro- and nanofabrication methods to integrate sensors to the material of choice can be avoided. This benefit provides a means to interrogate the state of materials in extreme environments without concern of the sensor being modified; as we'll discuss later, it turns out that ultra-pressure environments lead to some difficulties for optical probing which are ill-discussed in literature. Second, the ultra-short timescales of these pulses dictate the measurement's temporal resolution. When monitoring behavior of a material with continuous-wave lasers, the temporal resolution is generally dictated by the measuring electronics. For example, if the absorbance or reflectance of a material changes due to temperature, the observed change in this behavior is limited by the rate of which the photodetector and oscilloscope can detect such changes. In contrast, for USPs, the detectors/electronics observe an impulse, delta-function-like response – the amplitude of this pulse is directly proportional to the reflectance. In such a case, this single value of reflectance has a temporal resolution equivalent to the *laser* pulse width: Any "smearing" of this delta function is known to be the result of the electronics. Generally, for the works in this section of the document, our lasers have pulse durations less than 100

femtoseconds. This provides the ability to observe events with a time resolution *faster* than typical fusion rates (~1 ps).

Section overview

Our investigations into the use of these USPs for the stimulation and detection of AHE events are described in the sections below. These sections are as follows:

- USP1. Stimulation methods
- USP1a. Single pulse stimulation
- USP1b. Pulse train stimulation
- USP2. Detection methods
- USP2a. Transient Reflectivity
- USP2b. Archaeology

USP1: Stimulation Methods

As discussed above, USPs provide a unique method of stimulating materials: These pulses can deliver massive amounts of energy on timescales *faster* than atomic motion and electronic equilibration. Thus, these pulses provide one of the only methods to induce **non-thermal stimulation** of materials. Generally, Callisto Research's efforts investigated various flavors of *thermal* stimulation; different ways of delivering heat and monitoring for anomalous heat production via nuclear events. In our USP experiments, however, the pulses' ability to deliver energy at timescales *faster* than thermalization of electrons and phonons (vibrations of the lattice/atoms) provides our only look into non-thermal stimulation.

In the next two sections, we will look at our work on UV, visible, and near-infrared wavelength laser pulses (250 – 1200 nm) for such non-thermal stimulation. These efforts all surround the notion of non-thermal processes via direct stimulation of *electrons* in the material. In a later section, Terahertz, we manipulate these USPs to produce intense terahertz pulses, thus providing a look into direct stimulation of *phonons* in the material.

USP1a: Single pulse stimulation

In most of our experiments, we look at the effect of a *single* laser pulse that has a duration of less than 100 femtoseconds, or an array of pulses that are sufficiently spaced in time that they are independent and do not lead to accumulative behavior. To understand the effect of these pulses on

a PdD_x sample and the corresponding "non-thermal" behavior, we can turn to the two-temperature model (TTM)[30].

The TTM describes the material response when subjected to USPs with relatively high accuracy and is widely used throughout literature to understand this behavior in metals. The premise of the TTM is that when a pulse of light interacts with a metal, the high electron density of the material screens the pulse; this screening is what causes high reflectivity of metals. This screening works by the electrons oscillating in-phase with the pulse, causing the pulse to reflect. However, the oscillatory motion of the electrons causes them to gain some amount of energy; we can describe this energy gained by an electron temperature. In other words, when a USP interacts with a metal, it causes the electrons to heat up. In contrast, during this interaction, the lattice remains cold as the pulse was "screened" by the electrons; thus, the atoms themselves have not gained any energy and the lattice temperature is unchanged. During this time, the material is in a non-equilibrium, non-thermal state (i.e., the material isn't hot, only the electrons are!). After a finite amount of time, the electrons start to lose energy via collisions with atoms, causing the lattice to heat up. This behavior is shown in Fig. 1 below; the base code for the TTM can be found in **BE1209** and is used frequently in later experiments.

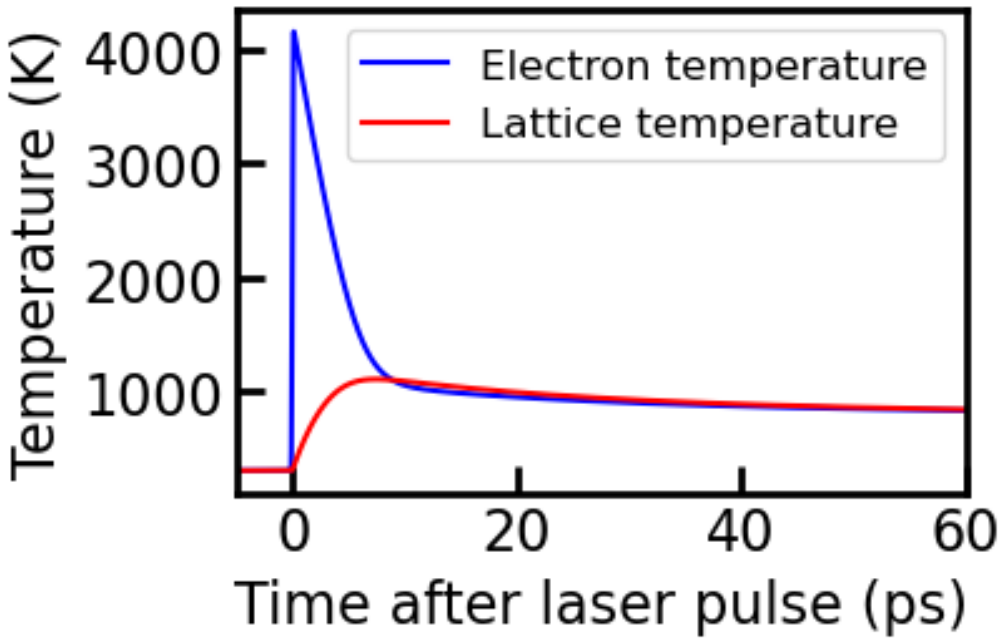

Figure 1: Electron and lattice temperatures following a 100-femtosecond laser pulse stimulating a Pd sample as calculated with the two-temperature model.

[30] Chen, J.K. *et al., International Journal of Heat and Mass Transfer* **49**, 307-316 (2006).

While this general TTM description works extremely well and is highly validated through experimental research in USPs, it is also extremely nuanced and only operates well in certain regimes or under certain assumptions. For example, the time that it takes for electrons to equilibrate with the lattice is proportional to the electron-phonon coupling factor, a generally intrinsic property of materials. However, knowledge of this material constant is determined by fitting the TTM to experimental data. As shown later, we determine this constant for PdD_x in our experiments. Another complication is that the *type* of USP that interacts with the sample can drastically change the behavior of this TTM process. For example, **by changing the wavelength of light, we intrinsically modify the way in which light interacts with the metal**.

Above, we stated that electrons screen the incident light pulse in metals. This is absolutely true, but only for certain wavelengths of light. At shorter wavelengths (higher photon energies), the electrons in metals can undergo *interband transitions*. This occurs by the wavelength of light causing an electron to jump from the valence band to the conduction band of the metal; this is the cause of non-silver colors of metals such as Au and Cu. In complex metals, this transition from oscillatory behavior to electronic transitions can be ill-defined, where many transition states exist through visible wavelengths[31]; this is the case for Pd and PdD_x. This complication, paired with the lack of theory surrounding AHE, suggests that *all* electronic transitions need to be considered.

While much of our work centers around either 800 nm or 400 nm stimulation/detection wavelengths, we also pursued these electronic transitions through the use of an OCPCA system (Optical Parametric Chirped Pulse Amplification). At a high-level, this is effectively a *tunable-wavelength* femtosecond laser system, capable of producing <100 femtosecond laser pulses (generally closer to ~35 fs), with tunability from 260 to 950 nm. This range allowed us to stimulate and investigate across nearly 5 eV of transition states. The relative energy levels and wavelength spectra of this system are outlined in **BE1235**.

USP1b. Pulse train stimulation

In our single pulse studies, the focus was on non-thermal stimulation via excitation of electrons. In parallel, we developed a method to investigate phonon-resonant stimulation using visible-wavelength USPs (again, later, we investigated the use of resonant THz laser pulses for an alternative approach to this hypothesis). The logic in this experimental thrust is as follows:

One hypothesis for AHE is that the deuterons within PdD_x oscillate "into" each other and undergo fusion. The exact details of this are, of course, vague due to a lack of sufficient mathematical theory. However, it is worth noting that atoms within a lattice are *always* oscillating; these collective oscillations are referred to as phonons. For any two-atom crystal basis (e.g., Pd + D), the material can support *optical* phonons, which are out-of-phase atomic vibrations. At a basic level, this arises from the mass mismatch between the two different atoms. These are referred to as optical phonons, as the frequency for these vibrations typically lies within optically accessible

[31] Lin, Z. *et al., Physical Review B* **77**, 075133 (2008).

frequency ranges; in many cases, these vibrations can induce direct absorption of light. For PdD_x, it has been established by both experimental neutron scattering and first-principal calculations that this phonon frequency lies around 10-14 THz. The hypothesis put forth toward AHE was specifically that *stimulation* of this phonon may cause sufficient oscillatory motion to cause deuterons to reach close enough proximities to undergo fusion.

Figure 2 below provides a visual contrast between acoustic phonons, which are the primary *heat* carriers in materials and are the modes that are stimulated in *thermal* stimulation methods, and these optical phonons investigated here, which are only weakly stimulated through thermal processes.

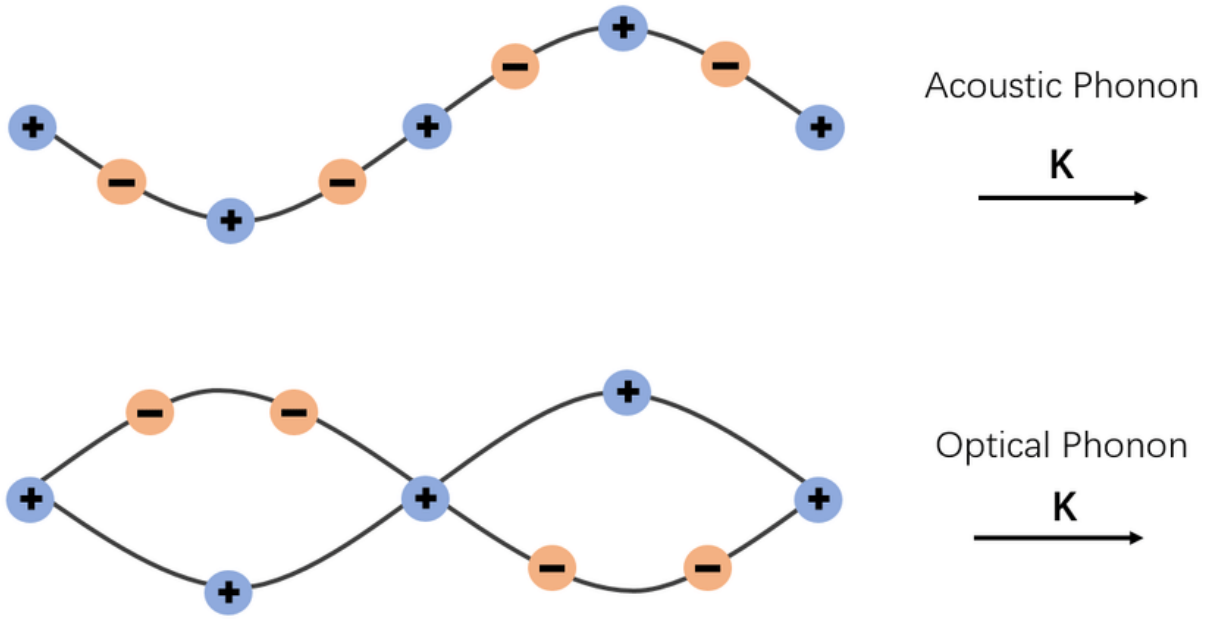

Figure 2: 1D visualization of (top) acoustic phonons and (bottom) optical phonons. One can envision the negative ions as Pd atoms and the positive ions as deuterons within the lattice. In both our "pulse train" and Terahertz stimulation efforts, the objective is to directly stimulate these out-of-phase optical modes in PdD_x, as acoustic phonons are sufficiently stimulated through thermal stimulation approaches.

To access this ~14 THz optical mode via *visible,* non-resonant USPs, we developed what we refer to as "pulse train" stimulation, where a train of ~35 fs optical pulses are separated by a time of $(14\ \text{THz})^{-1} \sim 70$ fs. This provides energy delivered to the lattice in-resonance with the motion of this optical mode, and resonant stimulation is a known method of increasing the amplitude of any oscillatory motion; does this increase in optical mode amplitude induce AHE?

These pulse trains are produced by leveraging the large frequency bandwidth of a USP. Due to the uncertainty principle, **the shorter a laser pulse, the more wavelengths/frequencies** (larger

bandwidth) it must contain[32]. In other words, when one refers to an 800 nm, 35 fs laser pulse, they really mean a ~770-830 nm laser pulse! The temporal shape of the USP is simply the Fourier transform of the sum of the frequencies composing the laser pulse; for an ideal ("Fourier transform limited") laser pulse, the sum of these different frequencies equates to a Gaussian time-envelope and is what we use for single pulse stimulation studies. **By manipulating the different wavelengths composing the pulse, we can manipulate the temporal shape of the laser pulse**.

This manipulation is done by modulating the *phase* of each frequency component. While this can be achieved experimentally through a number of approaches (most common example being phase-shift masks[33]), we induce phase modulation through spatial-light modulation (specifically, we use a 4f spatial light modulation geometry, shown in Fig. 3 below). To do this, we "split" the various wavelengths spatially using a diffraction grating; this is akin to sending light through a prism, where each wavelength exits at a different position. The wavelengths are then reflected from a liquid crystal array that is programmed with a specific spatial pattern; similar to phase-shift masks, the liquid crystal causes varying degrees of interference and thus imposes different phases to each wavelength component. After reflection from the liquid-crystal array, the wavelengths are recombined on the diffraction grating; the new pulse now has the imposed frequency modulation and thus temporal modulation.

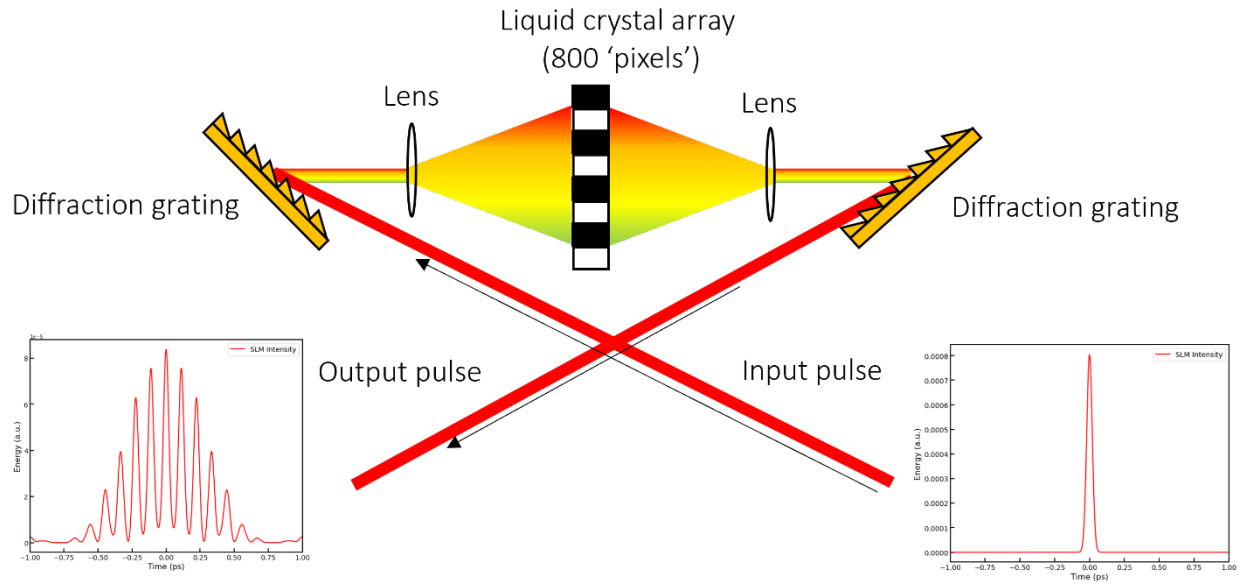

Figure 3: 4f spatial light modulation geometry (illustrated in a transmission layout) used to convert 35 fs laser pulses into "trains" of pulses at a given frequency.

Note, to generate "sharp" pulses in the time domain, the frequency domain requires sharp autocorrelations. This implies that we require *pseudo-random sequences of* phases in the frequency

[32] $\Delta E \Delta t > h$, where Δt is the pulse duration and $\Delta E = h\Delta f$, where f is the optical frequency; this optical frequency is inversely proportional to wavelength ($f = \frac{c}{\lambda}$).

[33] https://en.wikipedia.org/wiki/Phase-shift_mask

domain; non-random arrays will not produce sharp autocorrelations and thus not produce “clean” pulses in the time-domain. To do this, we introduced a maximum length sequence algorithm that generates the required “randomness” for phase modulation. These algorithms and the related development of this pulse train development are outlined in BE1231.

To observe the effects of these pulse trains on the material response, we implement our two-temperature model using a heat source equivalent to the calculated pulse array via our algorithm. An example of such is shown in Fig. 4 below, where the temperature can be shown to accumulate at all frequencies, but sharp transitions in temperature are observed at the high- and low-end of frequencies; these transitions correspond to different diffusion timescales within the material stack. These calculations allow us to separate *known* thermal accumulation effects from potential AHE effects. For example, one should certainly expect *more* damage at high pulse-train frequencies simply due to heat accumulation; this extent of additional damage can be pre-determined in the absence of AHE through such modeling approaches.

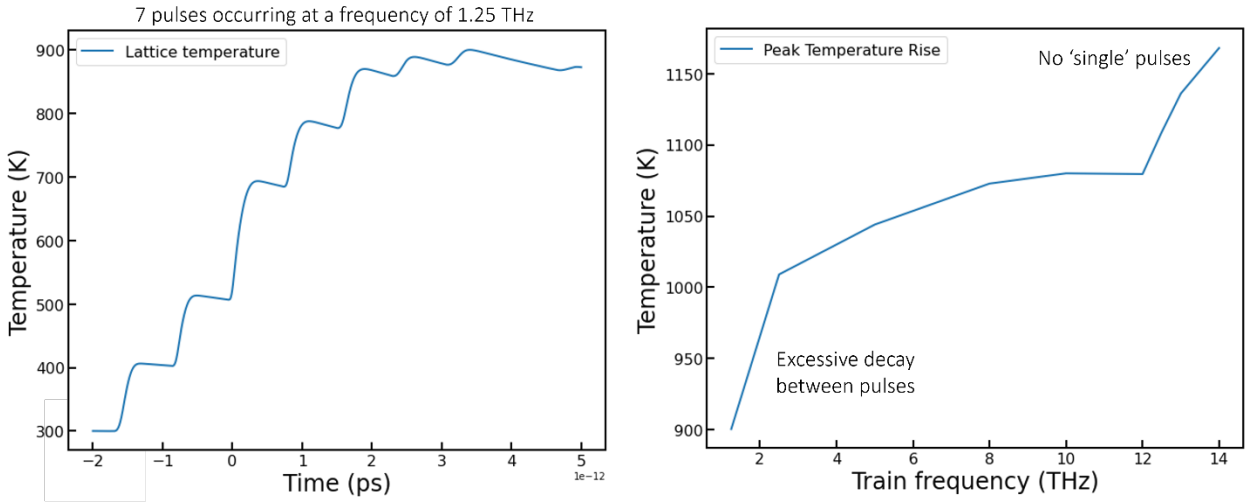

Figure 4: (Left) Example of TTM calculation using a 1.25 THz pulse train. (Right) The calculated peak temperature rise as a function of pulse-train frequency.

USP2: Detection methods

Due to the short timescale associated with USPs, most traditional thermometers do not have a time-response adequate for detection of the temperature rise associated with the short pulse (and thus not a sufficient temperature rise for AHE event detection!). To understand this aspect better, consider laser machining: Modern laser machining relies on ultrashort pulses for material removal because the pulse is capable of ablating material away faster than heat is deposited to the surrounding region. Thus, if a thermometer were placed nearby, it would observe negligible temperature rise; any anomalous heat events that occurred on a similar timescale would have

similar issues. Thus, choice in an adequate thermal sensor is critical to detecting our developed stimulation methods.

In our USP efforts, we rely on two primary methods for AHE detection: Transient reflectivity and Archaeology. In transient reflectivity (TR) we leverage a *second* USP that acts as an ultrafast thermometer, providing temporal resolution better than 100 fs. The second method, physical archaeology, primarily relies on observation of material damage due to a given laser pulse. In both cases, controls with protium are critical to separating laser-induced damage from AHE-induced damage. Importantly, the **ultrafast aspect of USPs eliminates the need for removing convective differences between the two isotopes of hydrogen**: The USP delivers and dissipates heat faster than convective timescales (~femtoseconds vs. microseconds). This greatly simplifies our analysis for both detection methods.

USP2a: Transient Reflectivity

Transient Reflectivity (TR) is an optical "pump-probe" technique that allows for thermal detection at ~mK temperature excursions without the need for micro- and nanofabrication methods or direct contact with the sample of interest. Generally, at least for metals such as Pd and PdD_x, the sample of interest can be directly stimulated/heated and directly measured using TR. This non-contact approach thus avoids the effects of thermal resistances associated with the thermometer itself or the thermometer/sample interface. To put this thermal resistance problem in perspective and highlight the benefits of TR, we can consider Fig. 5, which highlights a range of *interface* resistances between two dissimilar materials.

As shown, one can find that the thermal resistance associated with the interface alone can be equivalent to the addition of up to 100 nm of SiO_2 to the interface. Notably, when developing in-contact microscale thermometers, one will generally aim to minimize insulator thicknesses specifically to avoid this issue of mismatched temperatures between the thermometer and the sample of interest. In the case where one wants to interrogate the temperature of a metal such as Pd or PdD_x, these intermediate insulators are a requirement, and thus introduce not only their own intrinsic resistances, but *two* additional interfaces that impose a fundamental limit on the accuracy of the thermometry technique. Thus, the ability to eliminate these additional thermal resistances and *directly* interrogate the temperature of a sample of interest is a unique benefit to optical thermometry methods such as TR.

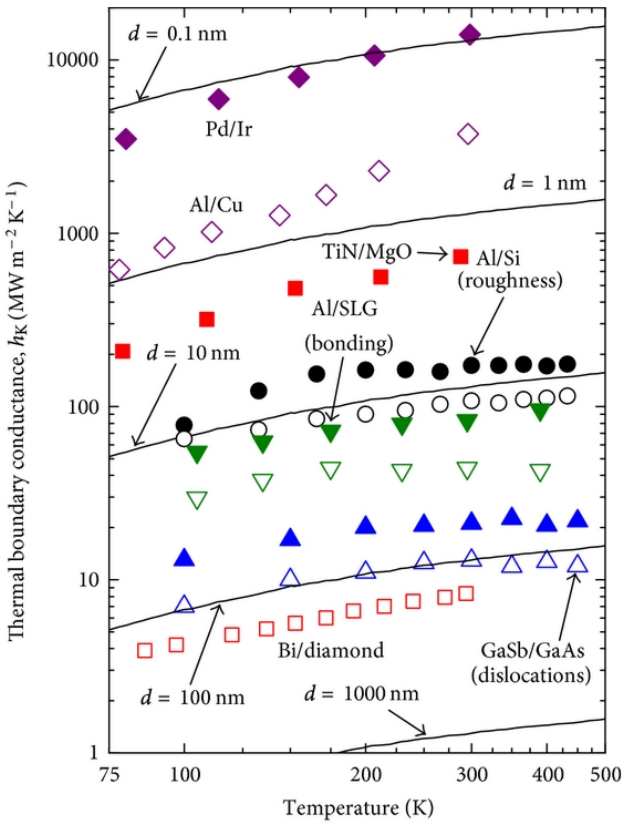

Figure 5: Thermal boundary conductance (~heat flow at material interfaces) for different material systems. The solid lines highlight the equivalent conductance if varying thicknesses of SiO_2 were added between the two materials, highlighting the ideation behind non-contact, optical thermometry.

TR, and other pump-probe methods, rely on using a laser pulse to stimulate/generate heat on a target surface while using a second laser pulse to measure the resultant temperature rise. In the case of our experiment, this is achieved by optically *splitting* a single laser pulse into two components; one portion of the beam is now the pump/stimulation pulse while the second beam acts as a probe pulse. To determine the time-evolution of this temperature rise induced by the stimulation pulse, we introduce a varying offset between the arrival time of the two pulses (i.e., the time-delay between the two). This is done using a retroreflecting mirror mounted to a motorized stage; as the mirror is mechanically moved to varying distances, the probe must travel the additional distance, d, before reaching the mirror, thus creating an additional time delay corresponding to $t_{delay} = \frac{2d}{c}$. The factor of two is produced from our experimental geometry in which the probe passes twice down the retroreflector. In our experiment, the pump pulse is frequency doubled to 400 nm while the probe pulse remains at the fundamental of 800 nm, allowing for spectral filtering of the two beams. A schematic representation of Transient Reflectivity is shown in Fig. 6 below.

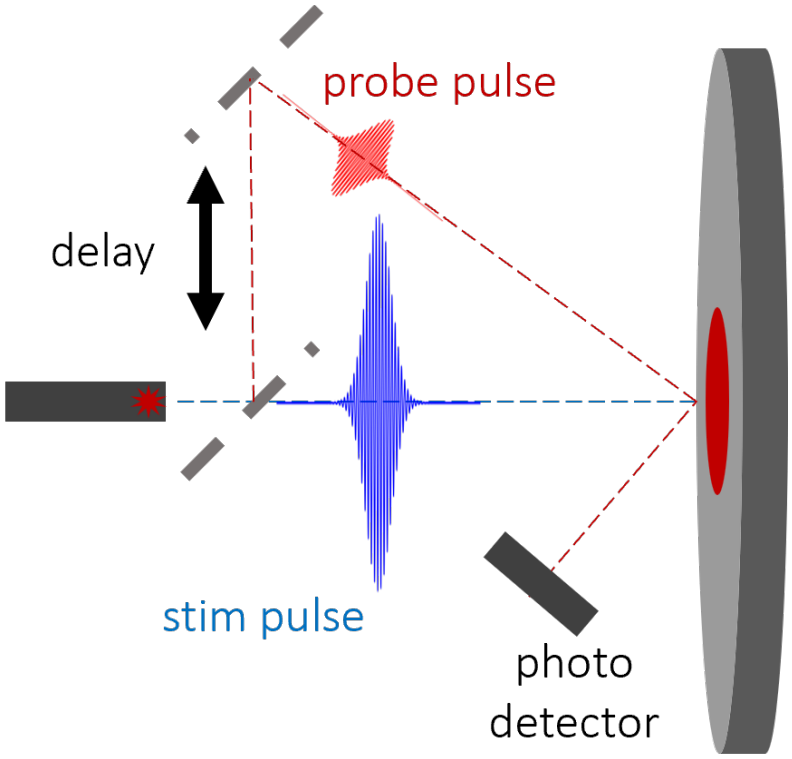

Figure 6: Schematic of Transient Reflectivity experiments. A single laser pulse is split into two components: A stimulation pulse and a probe pulse. The stimulation pulse creates a temperature rise on the sample surface while the probe pulse measures the resulting change in reflectivity, and thus temperature, of the sample surface. The temperature evolution in time is determined by repeating this process with varying path lengths of the probe pulse.

The objective in these TR experiments is, at a high-level, to look for AHE events through the observation of increased probe signal (i.e., temperature) following a stimulation pulse. This, in theory, may appear as an increased signal at all time-delays (which would be the case where AHE happens *during* the stimulation pulse and simply increases the average temperature/energy deposited) or a second event that occurs sometime after the stimulation pulse (i.e., if AHE happens 10 picoseconds following stimulation, then it will appear as though a second laser stimulated the sample).

During early investigations of AHE with Transient Reflectivity (USP2-1 through USP2-7 campaigns) several sample geometries and test conditions were investigated, including varying thicknesses of foils, cryogenic temperatures, loading conditions, and variations on the measurement hardware itself. The general objective in these experiments was to observe isotopic contrast – differences in the TR signal between PdH_x and PdD_x. However, multiple experimental concerns obfuscated the ability to reliably "look" for AHE events in these early investigations.

First, most of our early studies relied on the use of bulk sample geometries. However, materials with thicknesses exceeding a critical length scale tend to produce non-traditional TR signal due to

the non-equilibrium conditions associated with laser stimulation. A demonstration of this is shown below in Fig. 7, where we compare experimental TR measurements of a 100 nm vs. 20 nm PdD_x film under identical loading conditions (145 ksi D_2). As shown, when thicker films are used, there can be conditions in which the "hot electron peak" is not observed. This peak is due to non-equilibrium electrons that are initially excited by the pump pulse. After some time, generally a few picoseconds, these hot electrons lose energy to the lattice and the sample follows traditional heat conduction. However, in sufficiently thick films, these electrons can be ballistic and traverse into the depth of the thick layer, whereby they undergo thermalization away from the measurement surface. Similarly, the thermal decay of energy from the surface is dependent on the thickness of the film due to the aforementioned effects of thermal resistances at interfaces: In thick films of Pd, the material is highly thermally conductive and causes rapid decay of the induced temperature rise. However, in sufficiently thin films, not only are ballistic effects removed (they remain within the measurement volume), but heat conduction is limited by interfacial thermal resistances, causing the layer to stay hot for longer durations. This critical thickness is primarily dictated by the electron-phonon coupling factor of the metal.

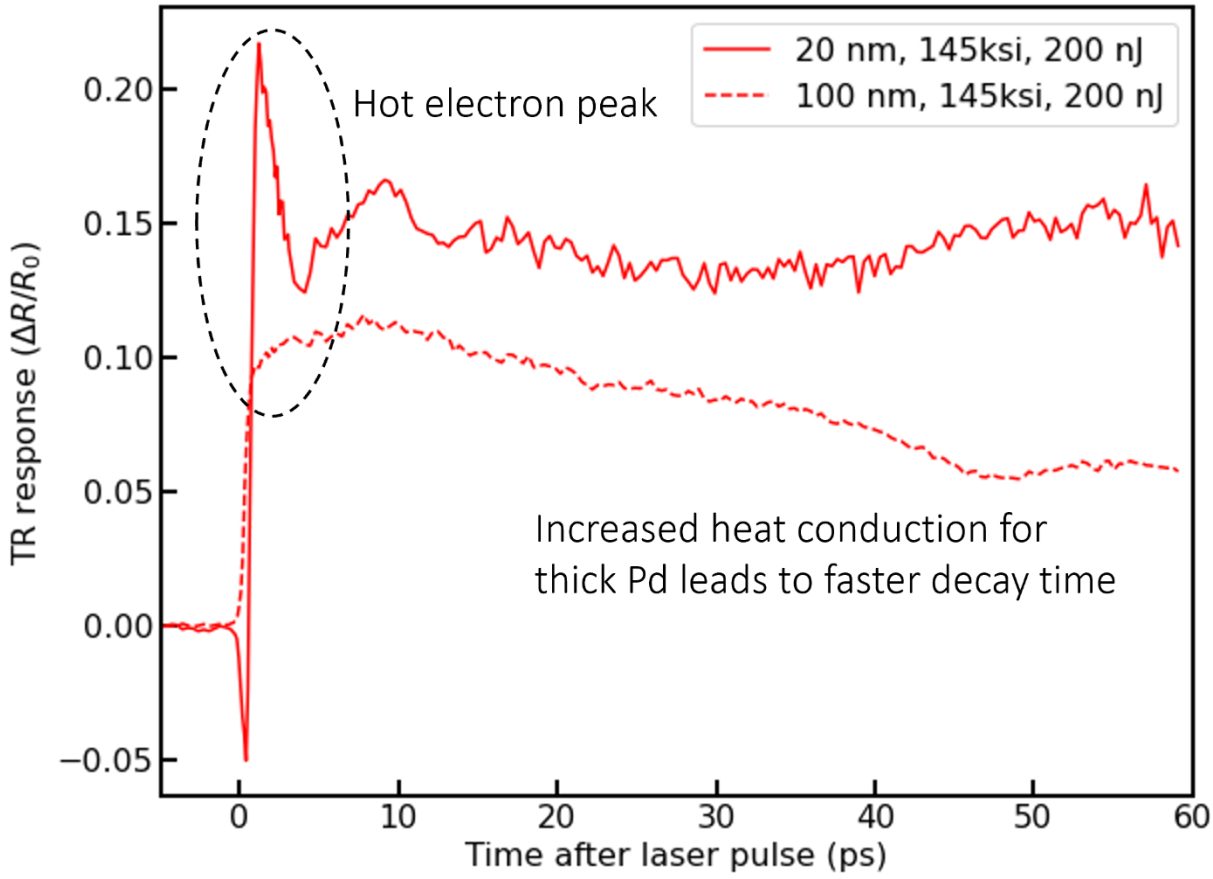

Figure 7: Comparison of experimental TR data for a 20 nm (solid line) and 100 nm (dashed line) PdD_x film at 145ksi pressure of D_2 gas. Contrast between the curves can be observed at nearly all time delays due to the non-equilibrium heat deposition from USP stimulation.

A second issue, as also highlighted in our Physical Archaeology section, is supercontinuum generation. At sufficiently high intensities, when USPs interact with dielectric media, the pulse can generate an array of non-linear optical processes. One of these, termed supercontinuum generation, leads to the production of white light. In other words, our 400 nm or 800 nm pulse can be spectrally broadened through the visible spectrum, taking a new spectral width that exceeds the filters. The issue with this process is that our TR experiment relies on spectral filtering of the two pulses; if one of them becomes broadband, the pulse will transmit through these spectral filters and produce anomalous signals in the photodetector. Second, this supercontinuum generation greatly distorts the spatial distribution of energy, causing local "hot spots" within the pulse, which can be interpreted as potential AHE events if not avoided. In our ultrapressure hardware, the sample is positioned behind a thick sapphire window – in our early experiments, the sample was simply too close to the window, thus requiring the USP to be highly focused when transmitting through the window. This leads to locally high intensities within the sapphire, creating supercontinuum, and leading to anomalous signals. This effect is shown below in Fig. 8.

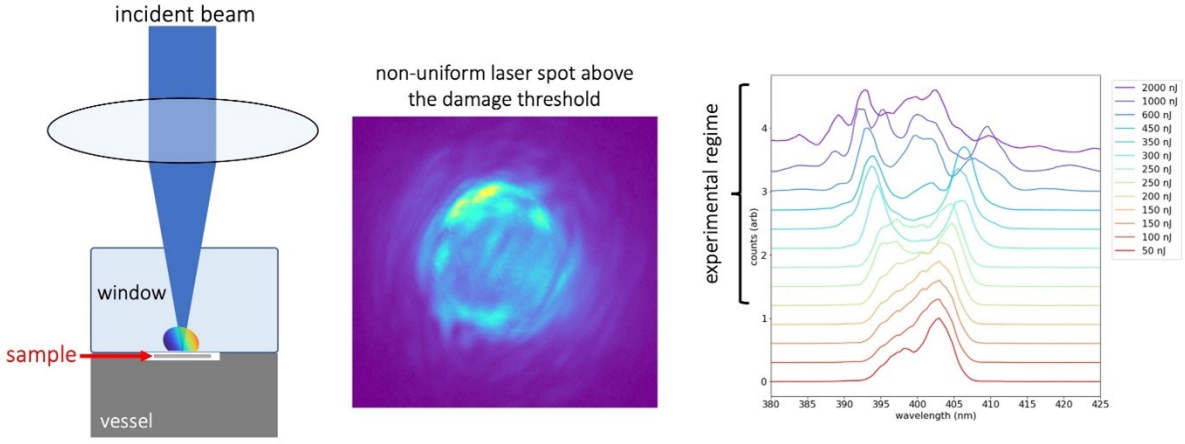

Figure 8: Supercontinuum generation from USP interactions with our high-pressure sapphire windows. (Left) Schematic of the high focusing conditions when the sample is placed too close to the window. (Middle) Image of an inhomogeneous laser spot due to this supercontinuum generation. (Right) shows the pump-pulse spectrum when supercontinuum occurs.

These two primary issues were resolved in experiments from USP2-8 onwards; more details on these types of artifacts that can produce "AHE-like" signals are discussed in USP-Appendix. Notably, upon resolving these issues, our TR experiments were highly repeatable and produced data consistent with two-temperature model calculations. Shortly thereafter, we observed highly reproducible isotopic contrast between PdD_x and PdH_x. An example of such contrast is shown in Fig. 9 below. As shown, one can observe that the data prior to a time-delay of zero (i.e., before the sample is stimulated), the two isotopes are identical. However, following stimulation with a pump pulse, PdD_x was observed to have *consistently* greater TR signals than its PdH_x counterpart.

Interestingly, this contrast was greater at intermediate loading conditions (<90%). As also shown in Fig. 9, increased pressures cause the two isotopes to converge, with only a small increase in TR signal for PdD_x.

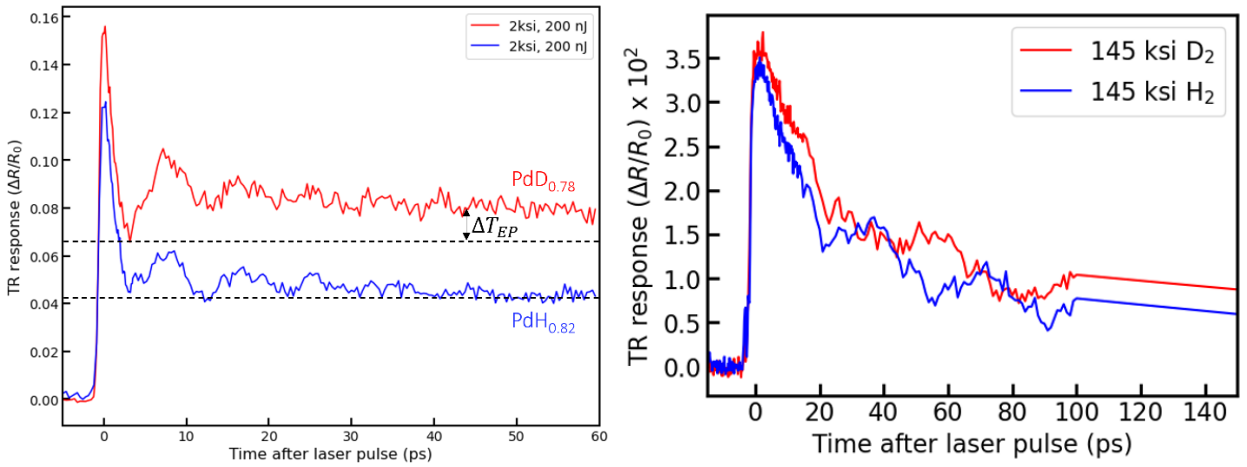

Figure 9: (Left) TR data for PdD_x (red) and PdH_x (blue) at pressures of 2 ksi and nominally 75% loading conditions; PdD_x was consistently observed to have a greater TR signal than its PdH_x counterpart. (Right) The same data acquired at 145ksi (~95% loading).

This isotopic contrast suggests one of two phenomena. First, the increased signal in PdD_x could suggest that the temperature is greater due to additional heat being generated within the sample; this could be the result of increased pump absorption in the metal or AHE events. The second possibility is that PdD_x produces a stronger change in reflectivity for a given increase in temperature. Different materials are known to produce varying thermoreflectance coefficients, and it is possible that PdD_x and PdH_x are simply "different materials" from a band structure perspective. This is certainly plausible given the known contrasts in electrical properties between the two isotopes.

Our first attempt at testing these hypotheses is shown in Fig. 10 below, where we performed Au controls in the two gas conditions. If similar behavior was observed here, it would indicate that the difference between deuterium and protium gas environments is responsible for the observed effect; notably, in the past, we had observed such isotopic differences due to collision-induced absorption in the mid-infrared. However, as shown in Fig. 10, we observed the *opposite* response, where H_2 gas produced a greater signal than D_2 gas. While certainly an isotopic difference, it suggests that the differences between PdD_x and PdH_x are *greater* than observed in our TR data!

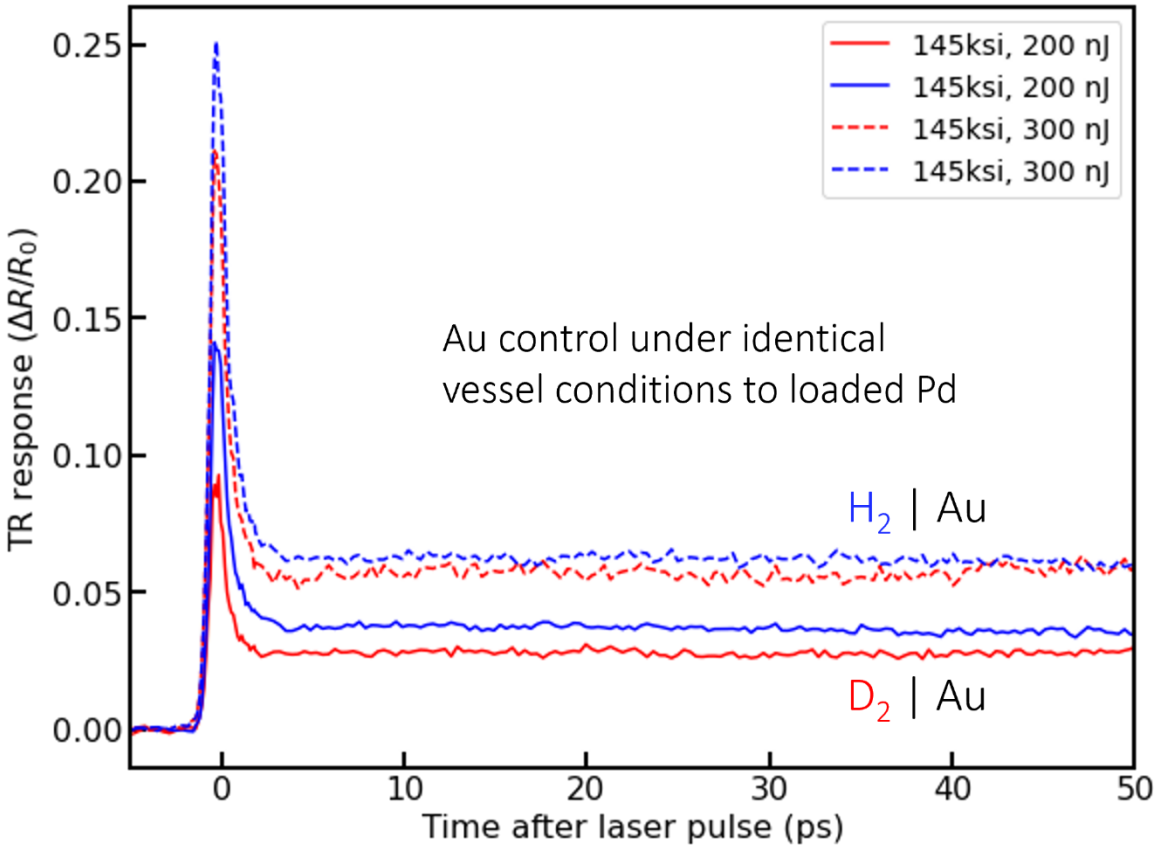

Figure 10: First attempt at resolving the observed isotopic contrast for PdDx vs. PdHx. In these experiments, we performed TR measurements on Au controls to isolate the role of optical differences between high pressure H_2 vs. high pressure D_2. However, we observe opposing behavior relative to our Pd experiments, where in the controls, H_2 is observed to produce a larger signal than D_2.

To further test these hypotheses, we rebuilt our TR experiment to allow for a new pump-probe geometry. Two major changes were made: First, we designed the setup to allow for measurements at much greater pump-probe time delays. This allows us to extend the datasets to timescales associated with heat diffusion and determine whether this observed isotopic contrast is simply the result of non-equilibrium behavior; it also allows us to look for potential AHE events at times much later than the pump stimulation. The second change was to allow us to pump and probe different sides of the material system. In doing so, by using an appropriate material stack, we can stimulate Pd, while measuring the temperature in an adjacent Au layer. Since we have determined the response of Au at elevated pressures and know Au does not produce AHE (Au doesn't load), this acts as an ideal optical thermometer. The concept of this is shown in Fig. 11 below.

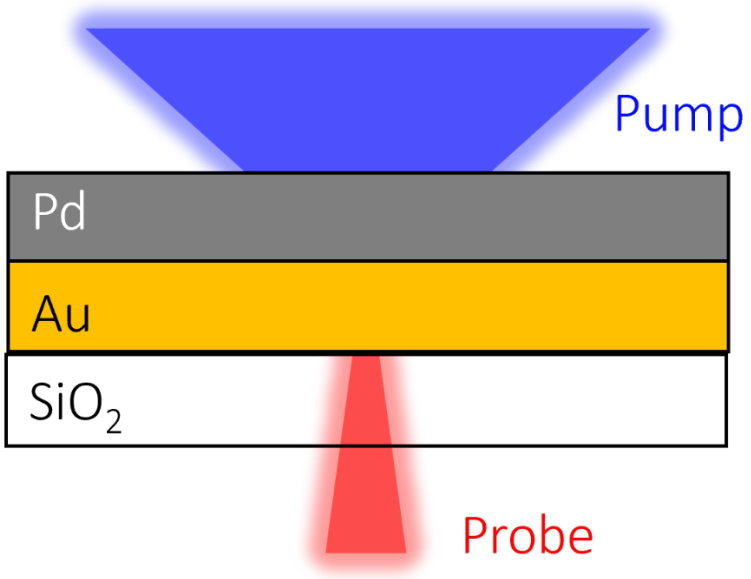

Figure 11: Schematic of revised TR setup to allow for stimulation of Pd while using Au as a constant optical thermometer.

While many experiments were conducted to verify the accuracy of this approach and eliminate any potential spurious signals not associated with AHE, the general conclusion is that the isotopic contrast *inverts* relative to pumping and probing the Pd alone. In other words, this experimental setup verifies that the observed isotopic contrast in which $PdD_x > PdH_x$ is solely due to differences in thermo-optical responses between the two material systems and is **not** associated with anomalous heat events. An example of these data is shown below in Fig. 12, where it can be observed that upon the probe interacting with Au following PdD_x/PdH_x stimulation, we no longer observe an increased signal for the deuterated metal. Two salient differences in these data from our prior TR experiments are due to the change in geometry. First, the slow rise in signal is because we are no longer stimulating the measured surface – heat must flow through Pd into Au before a measurable signal occurs; this slow rise is simply heat diffusion from the two layers. Second, the oscillations in the signal are primarily the result of Brillouin scattering within the SiO2 layer. When a rapid thermal excursion occurs, the thermally expanding metal launches an acoustic wave into the materials below; in this case, the Pd launches a wave into the Au/SiO2. This acoustic wave creates a local density gradient that is optically detectable on the probe beam; when the acoustic wave is distanced from the Au surface at integer multiples of the wavelength of light, interference will occur, causing local minima and maxima in the optical signal. In other words, the period of oscillation is found to match classical Brillouin scattering through $f_{osc} = \frac{2nv}{\lambda_{probe}}$, where n is the refractive index of the material (SiO_2), v is the sound velocity of the material, and λ_{probe} is the wavelength of the probe beam.

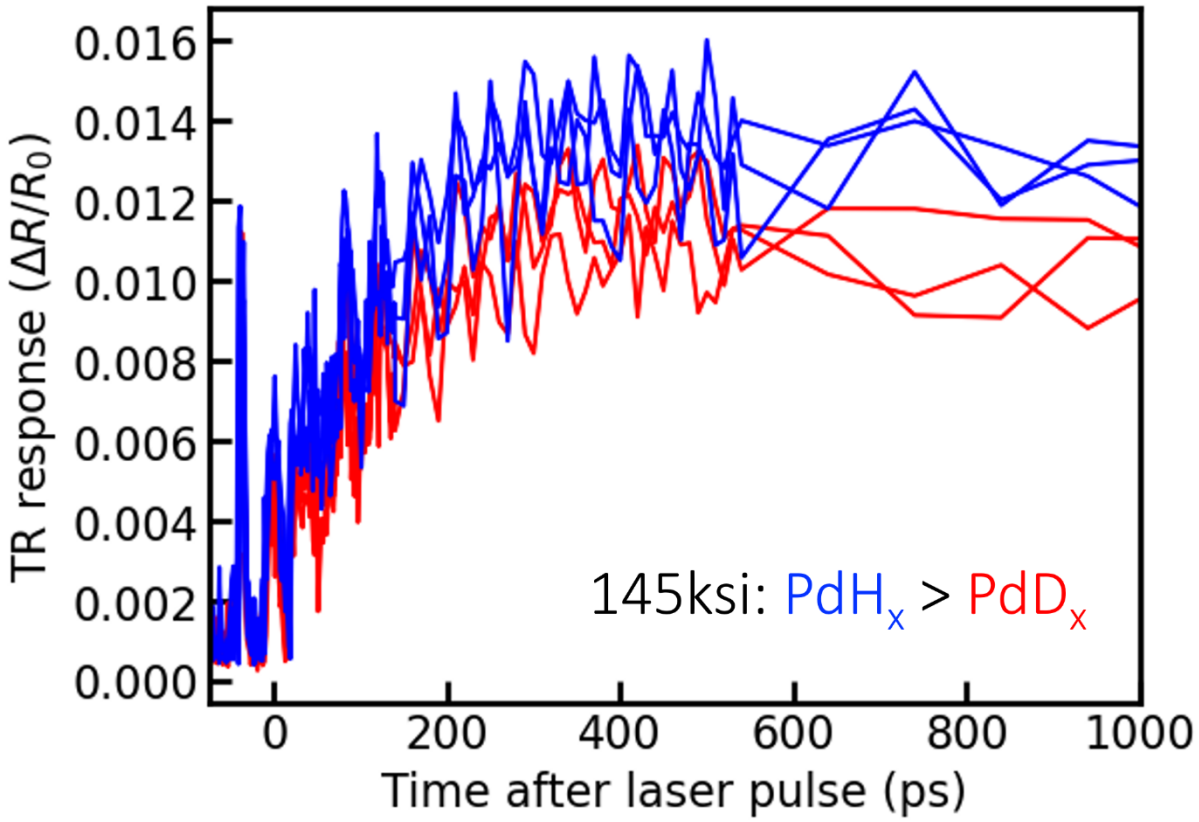

Figure 12: Experimental data from our revised TR setup in which the pump beam stimulates the Pd surface while the probe measures the thermal response of an Au film in direct contact with the Pd. The observed isotopic contrast is now consistent with control experiments on Au, in which the signal in PdH_x exceeds that of PdD_x. This experiment thus verifies that the original isotopic contrast was solely the result of differences in the material response functions.

Not only does this revised experiment verify a lack of AHE in PdD_x via laser stimulation, but it also suggests that optical probing is not a reliable method for AHE investigations when isotopic contrast is the sole method of potential AHE verification – the material response functions between PdH_x and PdD_x are simply too different for valid interpretation. Further, these experiments are repeated on rare-earth elements, such as Erbium, that allow for loadings near 300%. In no cases are AHE events observed.

USP2b. Archaeology

Our second method of looking for potential AHE events is through Archaeology. Opposed to TR, this method provides no direct *in situ* measurement of temperature rises. Rather, Archaeology detection relies on *ex situ*, *postmortem* investigations of material morphologies following

excitation. In other words, we compare the relative damage profiles between PdH_x and PdD_x to determine whether AHE occurred. The logic behind this is that the laser may induce some degree of damage to PdH_x, but if AHE events occurred, additional damage will have arisen due to the increased temperature excursion. In some cases, the laser is kept below the damage threshold, and the material is designed in such a way that the temperature rise associated with AHE should be sufficient to damage the material without any laser input. This structure size can be determined by a quick calculation on the temperature rise associated with a single AHE event; the specific heat of Pd (C_s) is 0.24 J g-1 K-1, the density (ρ) is 12.02 g cm-3, and we anticipate AHE to produce 24 MeV of energy internally. Assuming the material melts at the Pd melting temperature of 1830 K (the melting point is suppressed when loaded, so this *over*estimates the size threshold; sizes below this will melt once loaded if AHE occurs) the nanostructure volume to melt from a single AHE event is given by $V_{nanostructure} = \frac{24\ \text{MeV}}{1830\ \text{K} * C_s \rho} = 7.3 * 10^{-16}\ \text{cm}^3$. For a ~100 nm diameter pillar, this puts an upper length of 900 nm. In other words, for structures smaller than this critical volume, we can anticipate a single AHE event causing material melting to occur. Similarly, in the case where we use 20 nm Pd films, we can expect a single AHE event to induce a hole of at least 100 nm in the film, readily observable with electron microscopy methods.

At a first pass, one can use thin-film archaeology as a means of investigating potential AHE events. Generally, observing the *onset* energy of damage is the parameter of interest: If damage to a film is observed at lower intensities in PdD_x than PdH_x, it would be a potential indication that additional anomalous heat may have been generated within the deuteride. However, *discrete* measurements of this threshold are difficult and time-consuming: To accurately determine the potential addition of 24 MeV, one must vary the laser energy in increments of 24 MeV and find the onset of damage (i.e., a *massive* number of data points must be obtained). Further, the onset of damage is typically not observable: Damage takes the form of local melting and resolidification at low laser energies, which, at the nanoscale, is not observable until sufficient material modification has been performed (i.e., *observable* damage occurs much later than the *onset* of damage). In thin films, however, this energy threshold can be determined through a few (<10) laser shots on a single target through simple analytical modeling. Conveniently, for a Gaussian laser pulse, the threshold fluence (F_{th}, energy/unit area) is given by $D^2 = \omega_0^2 \ln\left(\frac{F}{F_{th}}\right)$, where D is the damage radius at a given fluence, F, and ω_0 is the beam waist. In other words, by plotting the *measured* damage area vs. incident laser energy, one can determine the threshold fluence via extrapolation.

We perform these thin film studies in a variety of shot conditions, including wavelengths spanning from 280 – 900 nm excitation, THz-tailored pulse trains, and excitation energies from well-below threshold to well-above threshold. An example of this data stream is shown in Fig. 13 below for pulse trains taken at 145 ksi of H_2 and D_2. In no cases do we observe statistically significant isotopic contrast with this approach.

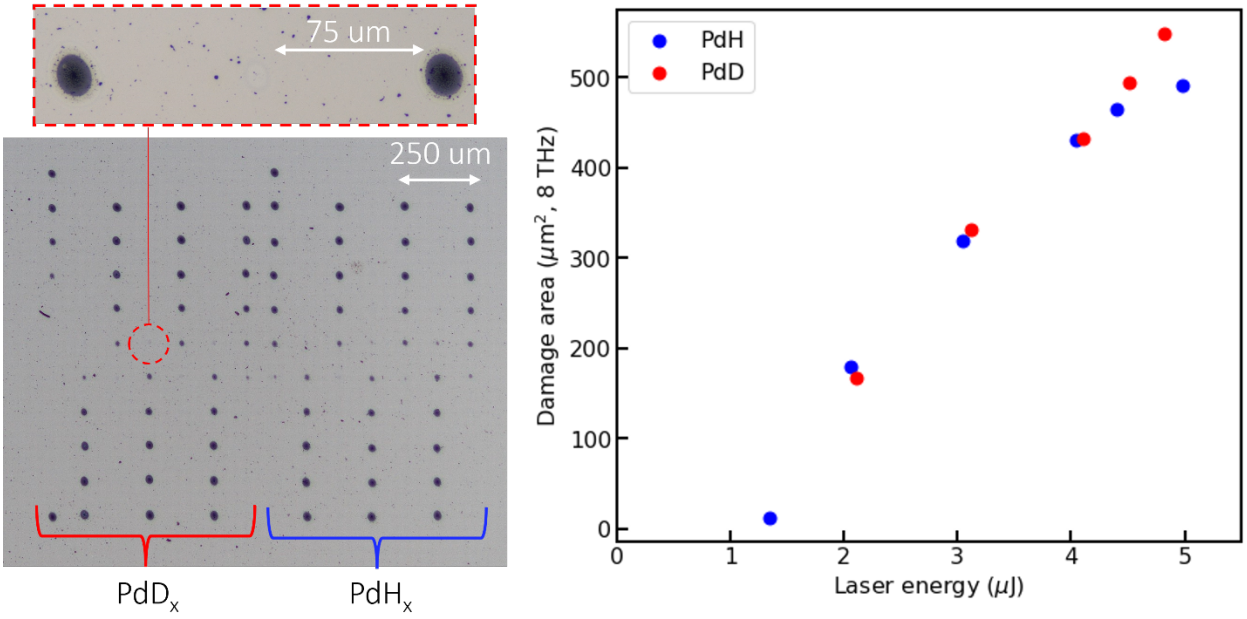

Figure 13: (Top left) Zoom in of damage to a 20 nm Pd film with a pulse train, (Left) Arrays of pulses for PdD_x and PdH_x with varying energies taken at different pulse train frequencies spanning from 0 to 12 THz and (Right) Example of the measured damage area vs. incident laser energy for a pulse train at 8 THz on PdD_x and PdH_x.

To more rigorously look for possible AHE events, we extend these thin film studies by performing post-mortem SEM imaging of nanofilm arrays. To test this USP stimulation at 100% loading conditions and consider the role of various materials/Pd alloys, we introduced a <100 fs pulse into our 400 ksi pressure vessel. As an additional comparison, we repeat this experiment using a long-duration thermal hold just below the melting temperature of the material of choice; these holds are achieved by introducing a continuous-wave (CW) laser. In this campaign, we thus intentionally remain *below* the damage threshold of the material due to the limited number of positions on a sample that can be obtained (i.e., our 400 ksi pressure vessel has a significantly reduced aperture relative to 150 ksi). Here, we look for >100 nm holes that form due to potential AHE events, as the laser is intentionally kept below the damage threshold. These films are 20 nm thick and span a range of material systems. This method allows for ***single-AHE event sensitivity.*** Table 1 highlights the results of this campaign; however, we note that no anomalous damage features of significance were observed or were not observed to be in isotopic contrast.

Table 1: Experiments performed at >400ksi with CW and USP stimulation with single event sensitivity.

Experiment ID	Sample ID	Material	Laser Source
BE3722	BD6828	Pd	3 kW, CW
BE3727	BD6829	Pd	3 kW, CW
BE3737	BD7171	$Pd_{0.75}Rh_{0.25}$	3 kW, CW

BE3739	BD7172	$Pd_{0.75}Rh_{0.25}$	3 kW, CW
BE3746	BD7318	$Pd_{0.75}Rh_{0.25}$	3 kW, CW
BE3750	BD7331	$Pd_{.75}Ni_{0.25}$	3 kW, CW
BE3752	BD7333	$Pd_{.75}Ni_{0.25}$	3 kW, CW
BE3752	BD7332	$Pd_{.75}Ni_{0.25}$	3 kW, CW
BE3756	BD7334	$Pd_{.75}Ni_{0.25}$	3 kW, CW
BE3757	BD7416	$Pd_{.75}B_{0.25}$	3 kW, CW
BE3761	BD7167	$Pd_{0.75}Rh_{0.25}$	3 kW, CW
BE3762	BD7418	$Pd_{.75}B_{0.25}$	3 kW, CW
BE3766	BD7417	$Pd_{.75}B_{0.25}$	3 kW, CW
BE3767	BD7418	$Pd_{.75}B_{0.25}$	3 kW, CW
BE3773	BD7635	$Pd_{.75}Pt_{0.25}$	3 kW, CW
BE3776	BD7636	$Pd_{.75}Pt_{0.25}$	3 kW, CW
BE3777	BD7637	$Pd_{.75}Pt_{0.25}$	3 kW, CW
BE3780	BD7508	$Pd_{.75}Ag_{0.25}$	3 kW, CW
BE3781	BD7509	$Pd_{.75}Ag_{0.25}$	3 kW, CW
BE3783	BD7510	$Pd_{.75}Ag_{0.25}$	3 kW, CW
BE3786	BD7639	$Pd_{.75}Pt_{0.25}$	3 kW, CW
BE3790	BD7511	$Pd_{.75}Ag_{0.25}$	Ekspla, USP
BE3794	BD7319	$Pd_{0.75}Rh_{0.25}$	Ekspla, USP
BE3795	BD7640	$Pd_{.75}Pt_{0.25}$	Ekspla, USP
BE3800	BD7512	$Pd_{.75}Ag_{0.25}$	Ekspla, USP
BE3803	BD7321	$Pd_{0.75}Rh_{0.25}$	Ekspla, USP
BE3805	BD7513	$Pd_{.75}Ag_{0.25}$	Ekspla, USP
BE3808	BD7322	$Pd_{0.75}Rh_{0.25}$	Ekspla, USP
BE3812	BD7356	$Pd_{.75}Pt_{0.25}$	Ekspla, USP
BE3815	BD7357	$Pd_{.75}Pt_{0.25}$	Ekspla, USP
BE3819	BD7335	$Pd_{.75}Ni_{0.25}$	Ekspla, USP
BE3821	BD7423	$Pd_{.75}B_{0.25}$	Ekspla, USP
BE3823	BD7422	$Pd_{.75}B_{0.25}$	Ekspla, USP
BE3828	BD7337	$Pd_{.75}Ni_{0.25}$	Ekspla, USP
BE3830	BD7426	$Pd_{.75}B_{0.25}$	Ekspla, USP
BE3831	BD7338	$Pd_{.75}Ni_{0.25}$	Ekspla, USP
BE3850	BD7324	$Pd_{0.75}Rh_{0.25}$	Ekspla, USP

Additionally, we performed experiments using nano-features designed to enhance light-matter interactions. Further, these were performed at conditions sufficient to achieve 100%, stoichiometric loading (>400 ksi). Finally, we also performed experiments on rare-earth deuterides/hydrides to achieve >300% loading conditions.

One of our original test structures used 8-sided pyramidal structures to allow for plasmonic excitation of the Pd. An example of these structures and their effect on the optical field is shown below in Fig. 14, where pyramidal structures with varying pitch (**p**) are shown; the color is a

representation of the electric-field enhancement due to strong light-matter coupling (i.e., plasmonic enhancement). This type of optical modeling played a large role in our choices of nanostructures for USP stimulation and, as described later, THz stimulation.

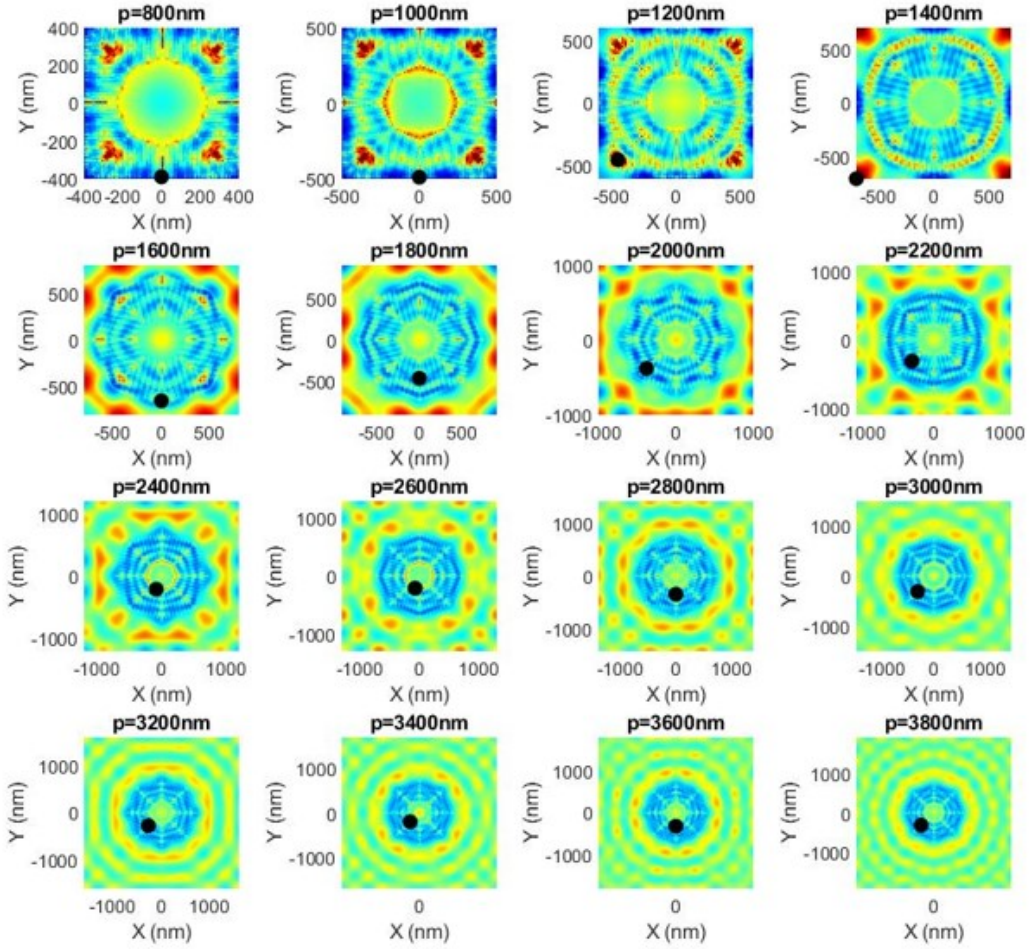

Figure 14: Electric field enhancement (color axis) for 8-sided pyramidal structures with varying pitch. The design wavelength was 400 nm. Calculations are performed using Lumerical.

Overall, there were a number of interesting phenomena/observations throughout this experimental campaign. One example, shown in Fig. 15, highlights nanoscale "jetting" that occurred due to USP stimulation of "bowties" (designed for internal plasmonic enhancement) at 145ksi. Interestingly, only bowties with this plasmonic enhancement displayed such features. To the best of our knowledge, no such process has been observed in literature and is truly unique. However, in no cases, including experiments performed at >400 ksi and achieving stoichiometric loading, nor geometries that allow for strong-field enhancement, do we observe isotopic contrast suggestive of

AHE. Including the bowties in Fig. 15, even these phenomena unique to our loaded Pd studies are found to occur in both deuteride and hydride alike.

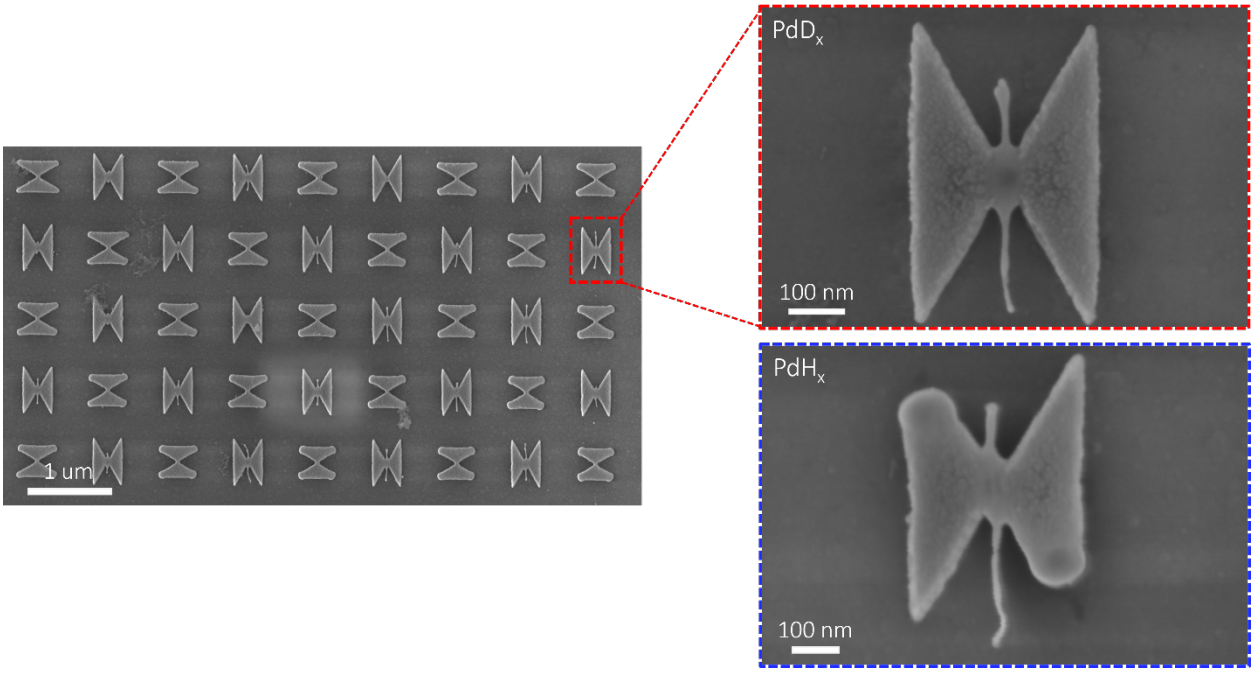

Figure 15: Example of nanostructures used for USP Archaeology studies. (Left) Overview image of "bowties" designed for plasmonic enhancement at the central point of two triangular structures. (Right) Shows unique "jetting" of melted material from the location of plasmonic enhancement; interestingly, this only occurs for orientations that undergo such enhancement. However, as shown, both deuteride (red) and hydride (blue) show these features.

USP-Appendix: Artifacts in TR measurements

TR "Imaging" for spatial variations due to mechanical stress on optical windows:

Figure 16: Concept and Example Result for Fixed-Delay 2-D Scan of Short Delay Feature

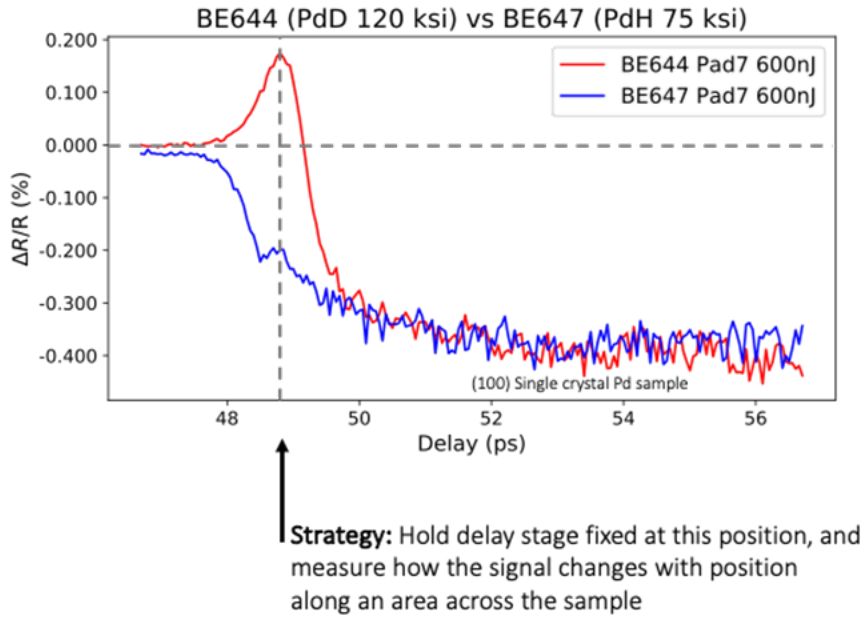

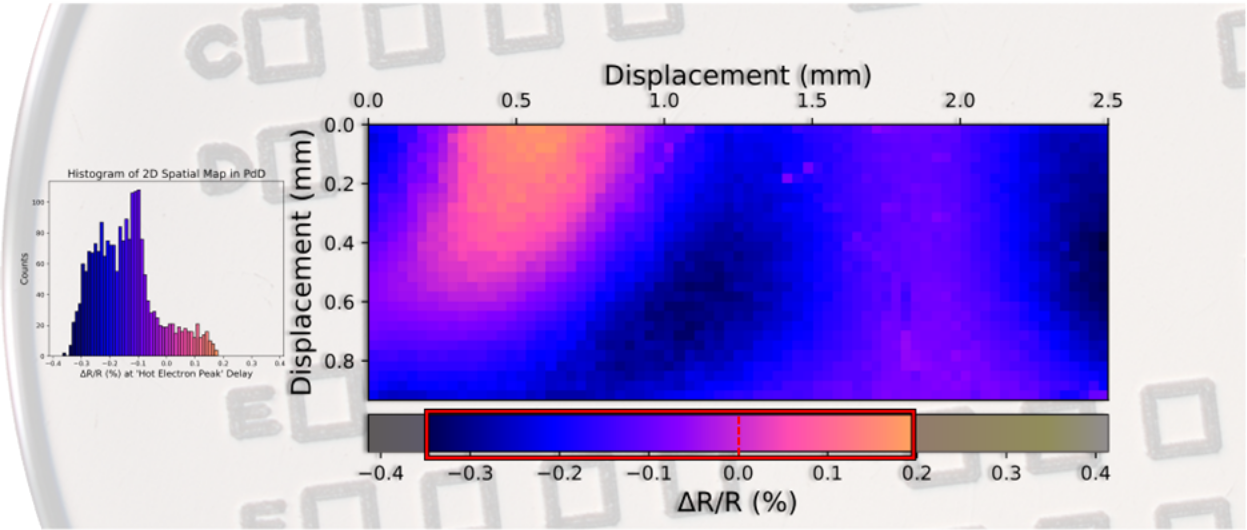

Concept for fixed-delay spatial scan. Delay stage is held at the position of interest, and the sample is scanned in two dimensions while the magnitude of the TR signal is recorded. Example map is shown overlain with an optical image of the single-crystal palladium sample. Histogram to the left indicates the spread of the feature of interest over the mapped area, and the range is highlighted in the color bar.

Transient reflectance data for the most part remained consistent between isotopes. However, it is worth noting that in early TR experiments, a sharp feature *occasionally* appeared at short pump-probe time delays of up to 2 picoseconds; this feature initially displayed as a form of isotopic contrast. To understand these differences, we performed fixed-delay two-dimensional scans to map this feature over the sample area in both isotopes. Figure 16 above details this approach and shows an example result.

In our investigations of this behavior, we identified several key observations:

1) The spatial variation only appears at high pressures.

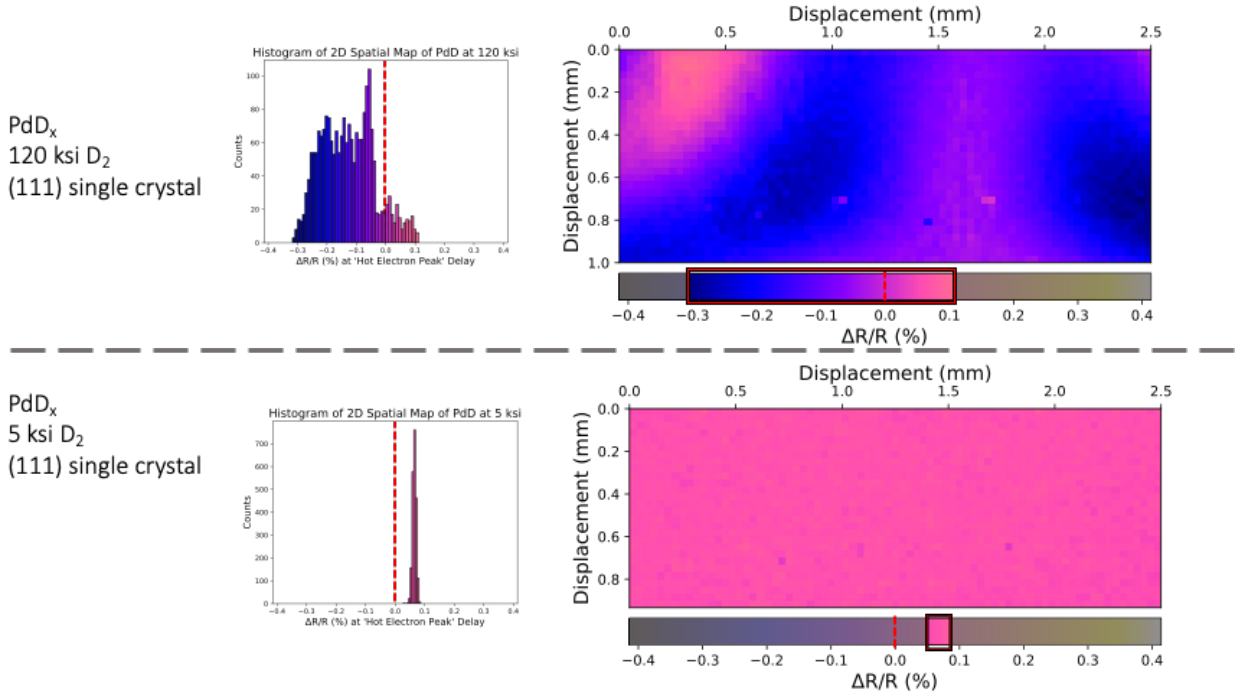

2) There appear to be isotopic differences in the short-delay feature, with larger positive magnitudes appearing in deuterium. This trend persists even at lower pressures when the distributions are narrower. Note: here we've matched *loading* rather than pressure.

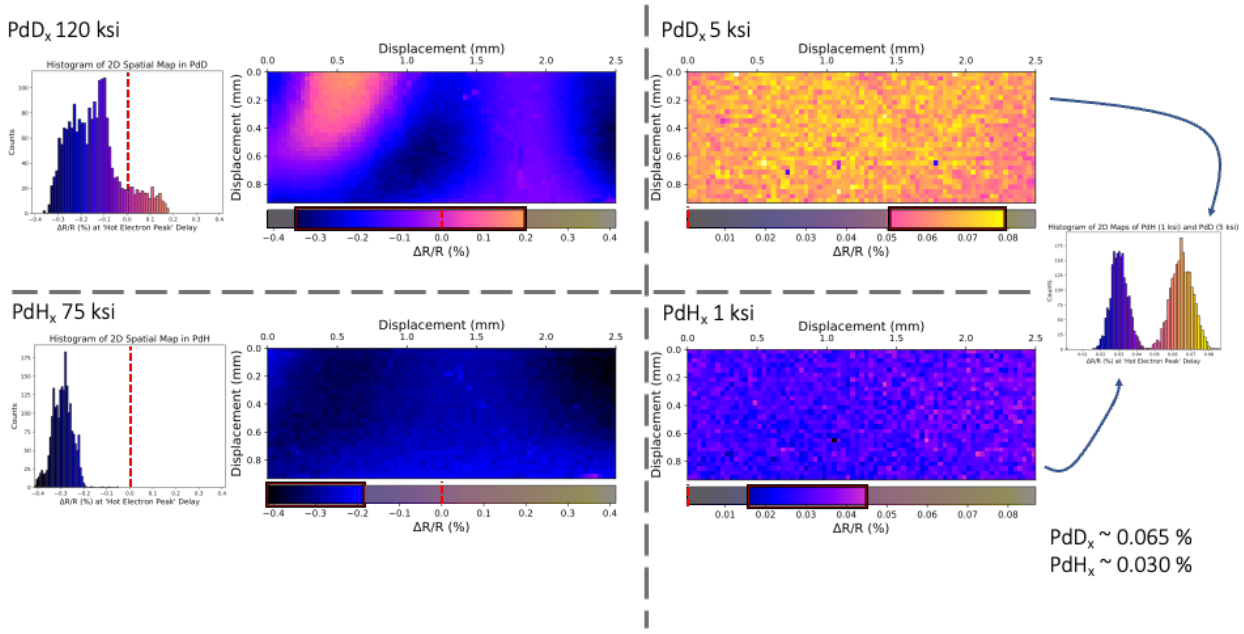

3) Nearly identical spatial patterns appear for different samples, which **indicates this is an apparatus effect rather than an interesting sample effect**.

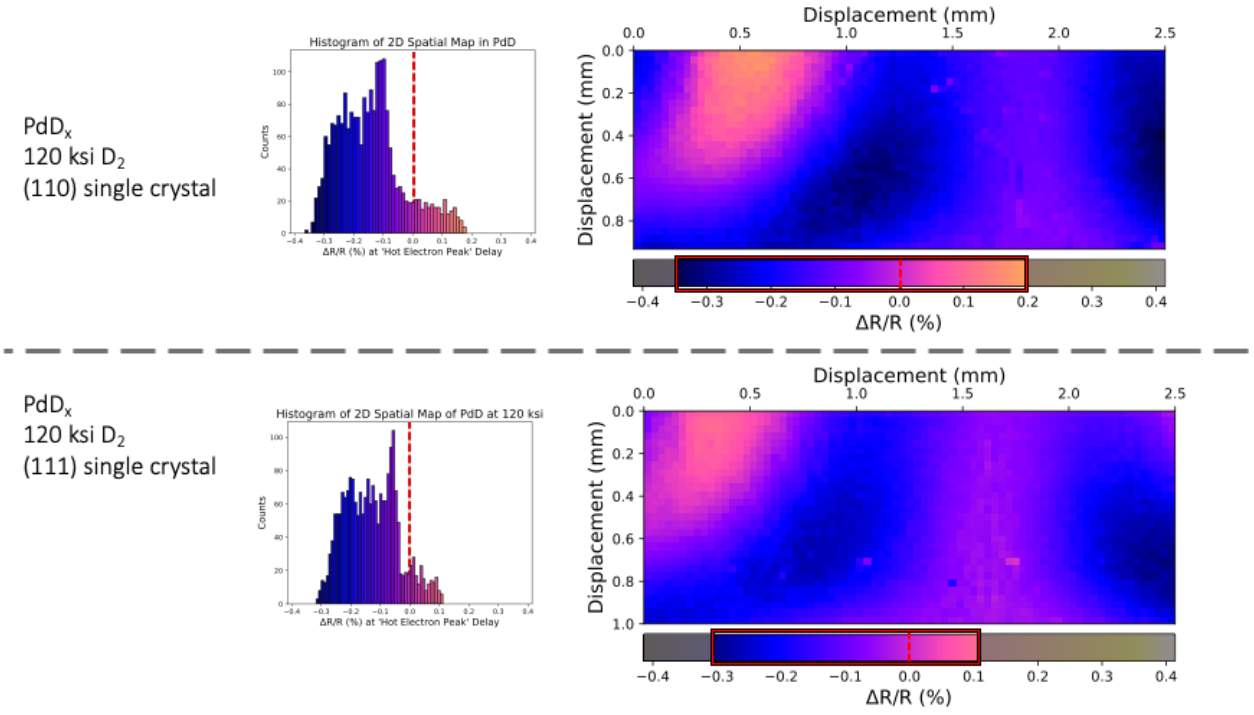

4) We also performed extensive measurements on gold samples, which do not load, and observed similar patterns. Our gold results are summarized below:
    - The TR signal at the peak delay shows spatial variation
        - Pattern ***depends on the apparatus***, not the sample
        - Pattern appears ***only at the peak delay***, not a few ps later
        - Pattern occurs ***only at high pressure, in H/D*** but not He
    - The Baseline 800 nm reflectance also shows spatial variation
        - Pattern ***depends on the apparatus***, not the sample
        - Pattern is ***not delay dependent***
        - Pattern occurs ***only at high pressure, in all gases***

As we demonstrate below, these observations are consistent with two different polarization shifts. Because transmission and reflection in different optics depends on polarization, shifts in the polarization couple directly into magnitude changes in our measured data. Our results indicate two different polarization shift mechanisms. One mechanism involves a stress dependent birefringence in the sapphire pressure windows, which shifts the baseline reflectance and results in a characteristic pattern based on the window geometry alone. The other mechanism is a polarization shift induced by the pump, in ultrapressure diatomic gases, which therefore occurs only shortly after the pump and probe occur at the same time. This explains the short-delay feature that is delay-dependent and that does not normalize away with the baseline reflectance.

Transmission Measurements in Ultrapressure Gas Reveal Polarization Effect

After determining that the spatial variation in the short-delay feature followed very similar patterns even after changing the sample, it became clear that the origin of the variation rested in the design of the apparatus. We performed a series of transmission measurements to explain the origin of the observed effect. As shown in Figure 17, we measured the energy transmission of each polarization component independently. We found that the total energy transmitted did not vary strongly with position, but the polarization did vary. Furthermore, the shape of the revealed pattern is consistent with the shape of the spatial variation in the short delay features in our TR data. This suggests that the sapphire window exhibits stress-dependent birefringence, leading to a spatially varying polarization shift in the transmitted light.

Figure 17: Polarization Varies Spatially but Transmitted Energy is Consistent

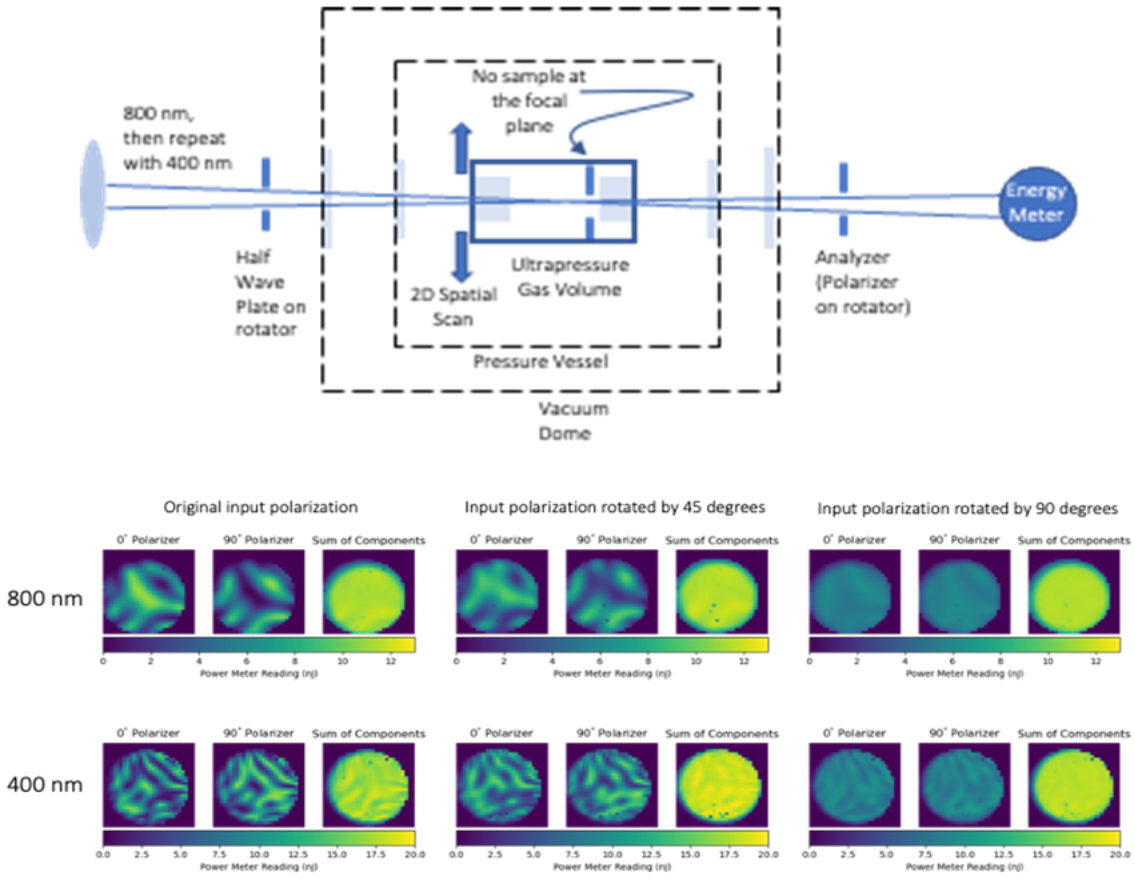

We measured the polarization of the transmitted probe and pump beams as we scanned over the whole ultrapressure bore. One scan was taken with the analyzer polarizer at 0 degrees, and then a second scan was taken with the analyzer at 90 degrees. These measurements were summed to demonstrate that the total energy remained consistent across the spatial scan, even though the polarization changed considerably. The measurement was repeated for three different input polarization angles.

Transient Transmittance Measurements Explain Short-Delay Feature as Gas Effect

The polarization shift due to the window alone is not enough to account for the variation we observe at short delays. Namely, the effect should normalize away in $\Delta R / R$ if the pump does not induce additional polarization change in the probe. To measure any induced pump-induced polarization change, we performed transient transmittance spectroscopy using an analyzer polarizer.

We found that indeed, with no sample present in the vessel, there is a polarization shift induced in the probe beam when it overlaps with the pump beam, as shown in Figure 18. We suggest this is some form of a Kerr effect in the ultrapressure gas, which is consistent with its appearance in diatomic gases but not in helium. This entirely explains our observed short-delay feature in transient reflectance data as a pump-induced polarization artifact.

Figure 18: Transient Transmittance Showing Pump-Induced Polarization Shift

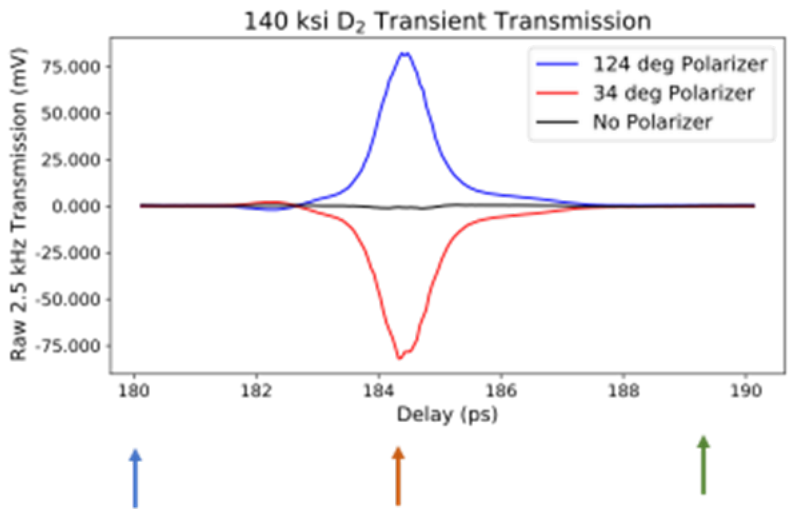

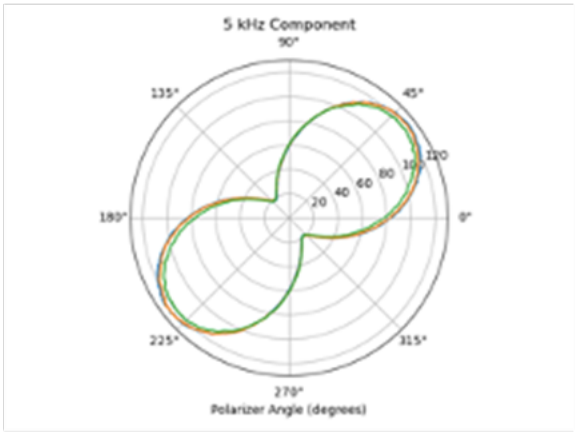

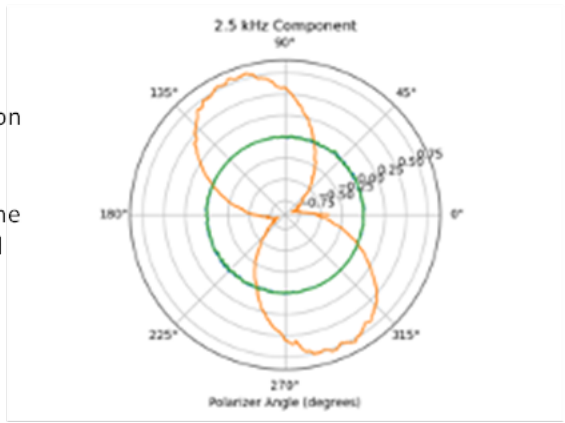

a) Transient transmittance data showing pump-induced polarization shift. This explains the variable short-delay feature in our transient reflectance data.
b) Bowtie plot showing the variation in the measured 5 kHz baseline transmitted probe light at three delay stage positions (indicated by the blue, orange, and green arrows on the TT plot) as the analyzer polarizer is rotated.
c) Bowtie plot showing the variation in the measured 2.5 kHz component in the transmitted probe light (i.e. the modulation due to interaction with the pump) as the analyzer polarizer is rotated. At the delay stage positions indicated in blue and green, there is no pump-related signal. However, at the delay stage position indicated in orange, the signal shows strong polarization dependence that is not the same as the baseline transmittance.

Isotopic Difference at Longer Delays Explained as an Interference Effect:

At pump-probe delays from 10 ps – 300 ps, we observed an isotopically different waveform in transient reflectance data, shown in Figure 19, which we ultimately explained as an interference

effect. The pump pulse superheats the surface and causes a shockwave to propagate out into the gas at the speed of sound. Part of the probe pulse then scatters off this wavefront and interferes with the reflected pulse. The interference is constructive when the wavefront has moved half a wavelength during the pump-probe delay time. The speed of sound in the dense gas depends both on pressure and on isotope, so the period of the observed waveform is different between deuterium and protium.

In the experiment shown, BE544, a palladium slug sample was elastically loaded up to 100 ksi in deuterium. Transient reflectance data was acquired at three different stimulation pump energies, at two different locations on the sample (labeled points A and B). The 10 ps – 300 ps waveform showed a magnitude that increased with pump energy, with a consistent period of ~100 ps. The waveform was consistent at both points measured. The sample was then elastically de-loaded, and then elastically loaded up to 100 ksi in protium. The measurements were repeated at two new locations (labeled Points C and D). The observed period in 100 ksi protium was ~80 ps.

Figure 19: Longer-Delay Oscillations Explained as an Interference Effect

The pump pulse superheats the surface of the palladium, which causes an acoustic shockwave to propagate into the gas. Probe light that scatters off of the wavefront can interfere with the reflected light when the right conditions are met. These conditions depend on the speed of sound, so the effect appears different between isotopes.

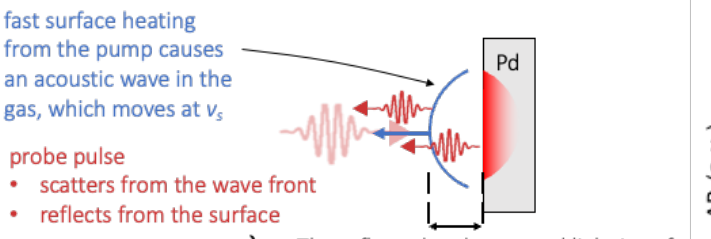

$$v_s \mathrm{T} = \frac{\lambda}{2n}$$

The reflected and scattered light interfere constructively when the wave front has moved a half wavelength during the delay, T, between pump and probe

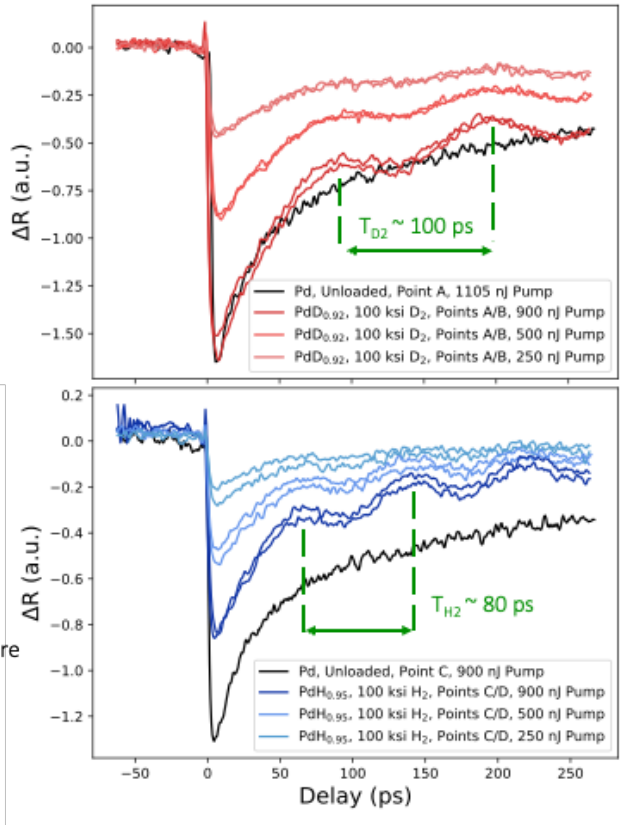

Argument for Focusing on Long Delay Features

Given the observed variation in short-delay features, we suggest that long-delays are far better indicators of the presence or absence of AHE. Admittedly, AHE is not expected to occur in precisely the same way for every stimulated pulse. However, any AHE that does occur would uniformly raise the temperature of the sample, crucially *for all times after the AHE event before complete temperature relaxation*. This means that even in an averaged measurement, some isotopic difference should be apparent at longer delays, before complete relaxation, unless AHE does not happen at all in the overwhelming majority of pulses; the Statistical Transient Reflectance technique discussed below was an attempt to address this possibility. Thus, later measurements focused on much longer delays than those presented above.

Statistical Transient Reflectance Measurement:

In conventional transient reflectance measurements, lock-in demodulation is used to characterize an average effect over thousands of pulses. However, because AHE is expected to be a rare event, it is possible or even likely that most individual pulses will not trigger AHE, and the averaged signal will not be measurably affected by the rare events. To address this concern, we developed a technique that collects raw, time-domain oscilloscope measurements of the photodiode response to each individual pulse. This still allows us to compute the average, for example by retroactively applying a digital lock-in filter, or by identifying a consistent quantity such as the peak height or area under the curve for each pulse. Additionally, however, we can quantify the distribution and compute quantities like the standard deviation that can give insight to the prevalence of rare outlier events.

We performed proof of concept experiments using this technique, but due to higher priorities this was not implemented in operational AHE experiments.

Figure 20: Proof of Concept Data for Statistical Transient Reflectance

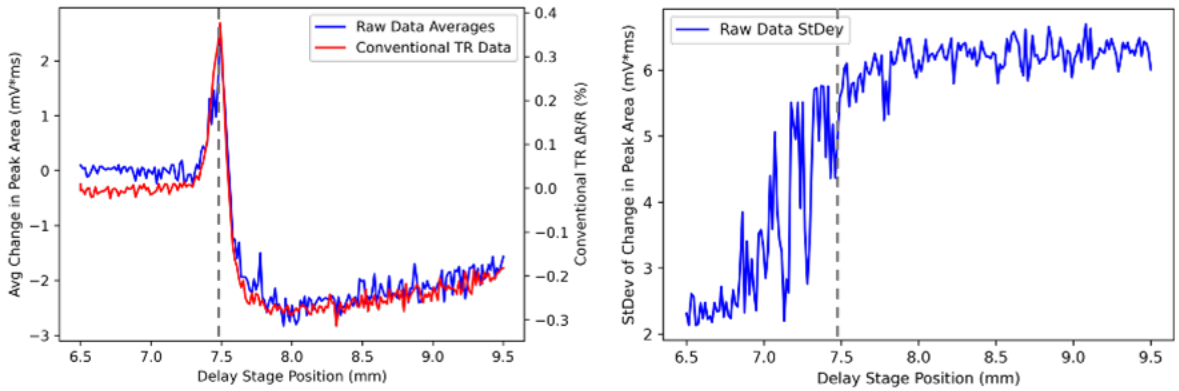

Conventional TR data is shown in red (right value axis) and is shown to be consistent with data extracted from computing the area under each pulse in a time domain oscilloscope trace (left value axis). Additionally, computing the area under each pulse in a time domain trace enables measurement of distributional quantities such as the standard deviation. Here, we see that the standard deviation increases when the probe arrives after the pump, which we suggest is the expected effect given the intensity noise in the pump pulses.